Using modal damping for full model transient analysis. Application to pantograph/catenary vibration

Jean Philippe Bianchi, Etienne Balmès, Guillaume Vermot Des Roches, Adrien Bobillot

Using modal damping for full model transient analysis. Application to pantograph/catenary vibration.

J.-P. Bianchi [1], **E. Balmes** [1,2], **G. Vermot des Roches**[1], **A. Bobillot** [3]
[1] SDTools
44, Rue Vergniaud, 75013, Paris, France
bianchi@sdtools.com balmes@sdtools.com vermot@sdtools.com
[2] Arts et Metiers ParisTech, Laboratoire PIMM (SDS), CNRS UMR 8006
151, boulevard de l'hôpital, 75013, Paris, France
[3] SNCF, Direction de l'Ingénierie
6, avenue François Mitterrand, 93574 La Plaine St Denis, France
adrien.bobillot@sncf.fr

Abstract
Experimentally, modal damping is known to allow a relatively accurate representation of damping for wide frequency ranges. For transient simulation of full finite element models, viscous damping is very often the only formulation that is associated with an acceptable computation time. In the absence of a proper material damping model, it is common to assume Rayleigh damping, where the viscous matrix is a linear combination of the mass and stiffness, or piece-wise Rayleigh damping. This representation very often results in modal damping ratios that do not correspond to the physical reality that can be tested. One thus introduces an implicit representation of the viscous matrix that allows transient time simulation with minor time penalty, while using a much more appropriate damping representation. Modal amplitudes are also considered to post-process time simulations and analyze damping levels. When studying vibrations induced by the passage of pantographs under a catenary, the high modal density of catenaries and the load moving over a large part of the model is a strong motivation to use full model transient analysis. Modal damping is shown to be a practical tool to analyze the properties of this complex system.

1 Introduction

Damping is the general term used to talk about physical dissipation mechanisms: material damping, friction, fluid/structure interaction, ... Dissipation in materials is linked to viscoelasticity or other non linear constitutive relations. Linear viscoelasticity [1, 2, 3] is classically represented through complex moduli, which do not have time domain equivalents, or internal states, which cannot easily be incorporated in standard FEM simulations. Friction typically occurs in joints that are either not modeled or not with sufficient detail to allow prediction.

As a result of these constraints, the physical mechanisms of damping are only modeled when such simulation is a primary objective. In other cases, one only seeks to reproduce system level behavior. In the frequency domain, one classically specifies modal damping ratio. While in the time domain Rayleigh damping is used. The objective of this paper is to demonstrate that modal damping can efficiently and usefully be used in time domain transient analysis.

OSCAR (Outil de Simulation du CAptage pour la Reconnaissance de défauts) is a pantograph-catenary dynamics software developed by SNCF and SDTools and certified with respect to the EN50318 standard. Its first objective is to provide signatures of defects and singularities (road bridges, turnouts, overlaps) to help

analyzing test data by extracting the relevant information. The second is to help designers to optimize existing or future OCL (Overhead Contact Lines). OSCAR uses a fully 3D FEM description of OCL geometries, including stagger, tensioned beam elements for the contact wire(s) (CW) and messenger wire(s) (MW), bar elements for steady arms and unilateral droppers. The pantograph can be modeled using both lumped mass or multi-body models with unilateral contact law.

Computing the static shape under tension and gravity loads is a first major difficulty. Starting from design data, that is the lengths of each component and tensions in CWs and MWs, tensions are applied first and non linear iterations are then used to converge on a static state. At this stage one can access to catenary elasticity, tension in each pretensioned element, static sag of the CW, modes, etc.

Pantograph description includes unilateral contact with the catenary, on one or multiple points when there are several CWs, and possibly non linearities such as end stops, friction, active control ... Time integration is performed using a classical implicit non linear Newmark scheme [4].

OSCAR provides the possibility of simulating the pantograph passage through a section overlap, which is a very attractive feature for assessing the different design possibilities. In this particular zone, the pantograph contacts one CW and then another, with a short period where it contacts both. One of the main issues for the modeling is then to have contact on each wire, taking into account the wire staggers.

Section 2 details the equations used for classical Rayleigh, modal and the proposed full model modal damping. Modal amplitudes are then defined to be used as post-processing tools in transient analysis.

In section 3, the proposed models are used to analyze the influence of damping on catenary vibrations using a simple pretensioned wire, an impact test on a full model and a standard pantograph passage.

2 Theory

2.1 Linear damping models

Viscous damping is a force that is proportional to velocity and leads to dynamic equations of the form

$$M\{\ddot{q(t)}\} + C\{\dot{q(t)}\} + K\{q(t)\} = \{f(t)\} \tag{1}$$

where the viscous damping matrix C is generally a symmetric semi-positive definite matrix thus ensuring a passive system.

Viscous damping is not physically representative of material damping, which is better represented by hysteretic models where the dissipation force is proportional to displacement, or friction, which tends to only depend on the direction of velocity. The use of viscous damping in time domain simulations should thus be considered as an equivalent approach. Viscous damping is however the only dissipation mechanism that is linear and thus low cost, so that the motivation to use it in models is very strong.

The most common viscous damping description is uniform Rayleigh model, where a linear combination of mass and stiffness matrices $C = \alpha[M] + \beta[K]$ is used. It is typically used when one has no real knowledge of damping: there are only two coefficients (or even one as $\alpha = 0$ is often considered) to adjust to match some response. More elaborate approaches use a piece-wise Rayleigh damping where distinct coefficients are used for various parts of the model

$$[C] = \sum_e \alpha_e[M_e] + \beta_e[K_e]. \tag{2}$$

The weighting α_e and β_e account for the fact that certain components are thought to be more dissipative than others and have dissipation proportional to the time derivative of displacement or deformation respectively.

Illustrations will be given in 3.2. A major limitation of this approach is that damping often occurs in junctions that are modeled as perfect and are thus not associated with matrices.

Real modeshapes $\{\phi_j\}$ and pulsations ω_j are solutions of the eigenvalue problem

$$(-\omega_j^2[M] + [K])\{\phi_j\} = \{0\}. \tag{3}$$

When taking all modes, one has the mass orthogonality conditions and can use the fact that a matrix and its inverse can be permuted to obtain the following relations

$$([\Phi]^T[M])[\Phi] = [\Phi]^T([M][\Phi]) = I = [\Phi]([\Phi]^T[M]) = ([M][\Phi])[\Phi]^T \tag{4}$$

One also has the stiffness orthogonality condition, which for mass normalized modes is given by

$$[\Phi]^T[K][\Phi] = \left[\backslash \omega_j^2 \backslash\right]. \tag{5}$$

Modal damping [5, 6, 7] corresponds to the assumption that the viscous damping matrix is diagonal in the real mode basis, that is to say that

$$[\Phi]^T[C][\Phi] = \left[\backslash 2\omega_j\zeta_j \backslash\right]. \tag{6}$$

where ζ_j is the modal damping ratio of mode j. Using orthonormalization conditions (4)-(5), one can easily show that for uniform Rayleigh damping, one has

$$\zeta_j = \frac{\alpha}{2}\frac{1}{\omega_j} + \frac{\beta}{2}\omega_j. \tag{7}$$

Damping proportional to mass cannot be applied to cases with rigid body modes, since they would have infinite damping, and is limited to damp the first few modes since the damping decreases with frequency. Damping proportional to stiffness increases linearly with frequency which rarely corresponds to the physical behavior, where damping ratios are mostly constant over large frequency range.

If modal damping is a valid assumption, the Modal Strain Energy method [8] can be used and leads for modeshape $\{\phi_j\}$ to

$$2\zeta_j\omega_j = \sum_e \alpha_e \left(\phi_j^T[M_e]\phi_j\right) + \beta_e \left(\phi_j^T[K_e]\phi_j\right) \tag{8}$$

In reality modes are really complex, so that the damping ratio is not associated with the real modeshape as assumed by the MSE method. As shown in [5, 7] and illustrated in figure 10, modal damping is however always a good approximation for well separated modes and often a close approximation otherwise.

An important consequence of this equation is that modes where most of the energy is concentrated in element group e will have a damping ratio given by $\frac{\alpha_e}{2}\frac{1}{\omega_j} + \frac{\beta_e}{2}\omega_j$. It also follows, as will be illustrated in figure 7, that piece-wise Rayleigh damping generates damping ratios that are limited by the various weighting coefficients.

In the modal basis, viscous damping is easily expressed as a diagonal matrix (6). Going back to the physical basis the modal diagonal matrix becomes full. Using (4), it clearly appears that $[\Phi]^{-1} = [\Phi]^T[M]$ and $[\Phi^T]^{-1} = [M][\Phi]$. One can thus invert (6) and obtain

$$[C] = [M\Phi]_{N\times N_m}\left[\backslash 2\zeta_j\omega_j \backslash\right]_{N_m\times N_m}[M\Phi]^T_{N_m\times N} \tag{9}$$

The equation is exact when all modes are kept but is typically applied using a truncated modal series of N_m modes. A key aspect of this simplification is that rows of $[\Phi]^{-1}$ are given by $\{\phi_j\}^T[M]$. The C matrix in (9) is full and thus too large for practical applications. For time simulations one however needs to compute $[C]\{v\}$ products, which can be organized as

$$[C]\{v\} = \left([M\Phi]\left(\left[\backslash 2\zeta_j\omega_j \backslash\right]\left([M\Phi]^T\{v\}\right)\right)\right). \tag{10}$$

which involves a full transposed matrix/vector product $[M\Phi]^T\{v\}$, a multiplication by a diagonal matrix and a second matrix vector products. One thus only stores $[M\Phi]$ for selected modes and uses BLAS (Basic Linear Algebra Subroutines) to perform these operations. These routines are now very well parallelized and very good performance can be achieved.

The number N_m of modes and associated damping coefficients, directly impact computation time. Part of the procedure is thus to select target modes that are of interest and combine with a Rayleigh model for the rest of frequencies. In that case, Rayleigh damping should be compensated in order to obtain desired modal damping ratios. For a desired $\hat{\zeta}_j$, one thus uses (10) with

$$2\zeta_j\omega_j = 2\hat{\zeta}_j\omega_j - \phi_j^T C_0 \phi_j \tag{11}$$

where C_0 is the Rayleigh damping. Compensation is exact if modal damping hypothesis (6) is verified and approximate otherwise.

2.2 Modal amplitudes and energies

An idea closely linked with modal damping is that modal amplitudes are quantities of direct interest in transient analysis. By definition of modal coordinates, the response can be described as a linear combination of modes

$$\{q(t)\} = [\Phi]\{\alpha(t)\} \tag{12}$$

where $\{\alpha(t)\}$ is the vector of the modal amplitudes. Using the inverse of $[\Phi]$ implied by (4), one finds

$$\{\alpha(t)\} = [M\Phi]^T\{q(t)\} \tag{13}$$

$$\{\dot{\alpha}(t)\} = [M\Phi]^T\{\dot{q}(t)\} \tag{14}$$

which can easily be computed either as a post-processing step if all components of q are saved or during the time simulation as a generalized sensor. This is a direct application of the modal sensor concept known in the active vibration control literature.

Modal energy is the mechanical energy associated with a given mode and is given by

$$Em_j(t) = \frac{1}{2}(\alpha_j(t)\phi_j^T K \alpha_j(t)\phi_j + \dot{\alpha}_j(t)\phi_j^T M \dot{\alpha}_j(t)\phi_j) = \frac{1}{2}(\omega_j^2\alpha_j^2 + \dot{\alpha}_j^2) \tag{15}$$

In modal coordinates, mass and stiffness are diagonal matrices. It thus clearly appears that the total mechanical energy is the sum of modal energies.

3 Validation

This section illustrates the use of modal coordinates and damping for transient analysis of catenaries. Section 3.1 uses a simple pretensioned wire to illustrate the use of modal energies and the modal damping properties of Rayleigh damping. In section 3.2 an impact test is used to show how modal damping ratio can be used to get the transient model to fit global behavior better. Finally section 3.3 illustrates how modal damping can be used to analyze full transient analyzes.

3.1 Pretensioned wire

The example of a simple wire is first considered to illustrate the relation between transient analysis and modal quantities. The model is a tensioned wire (l=60m, T=10kN) hung every 6m to springs (K=50kN). An initial

global Raleigh with $\alpha = 0$ and $\beta = 3.25e - 3$ is defined. The passage at a speed of 83m/s of a pantograph with mean contact force of 150 N is simulated.

The pantograph-catenary interaction is a moving load problem. Modal amplitudes and modal energies of the wire depend on modeshapes and modal energies can be used to analyze this dependence. Modes, see figure 1, can be separated into horizontal (5,7 and 9) and vertical modes (1,2,3,4,6,8 and 10). Only vertical modes are excited by the pantograph when sliding under the wire. This is directly confirmed by the maximum modal energies shown in the figure 1. In more complex cases, the sorting of modal energies can be used to identify excited modes. This is important for modal damping implementation, since the damping of modes that do not respond has no influence on the response.

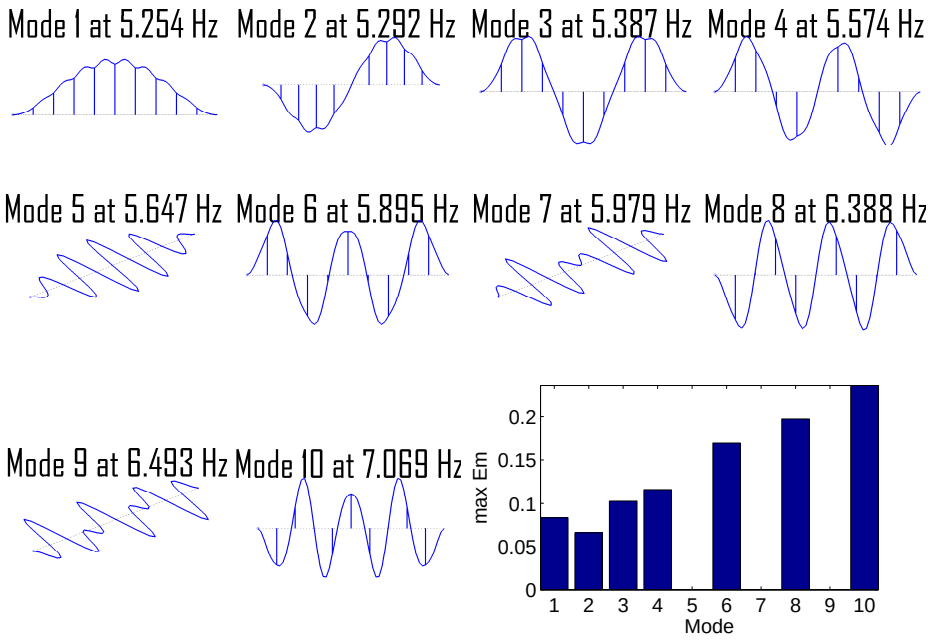

Figure 1: First 10 modes and corresponding maximum modal energy during pantograph passage.

To get a better understanding of how modal energies evolve, figure 2 compares modal energies through the passage and modeshapes using the same horizontal scale. A decrease of modal energies, when the pantograph is around the nodes of modes 2 and 3 is clearly visible. The fact that energies do not drop to zero indicates that decrease due to damping is not fast compared to the time that the pantograph takes to pass a modeshape node.

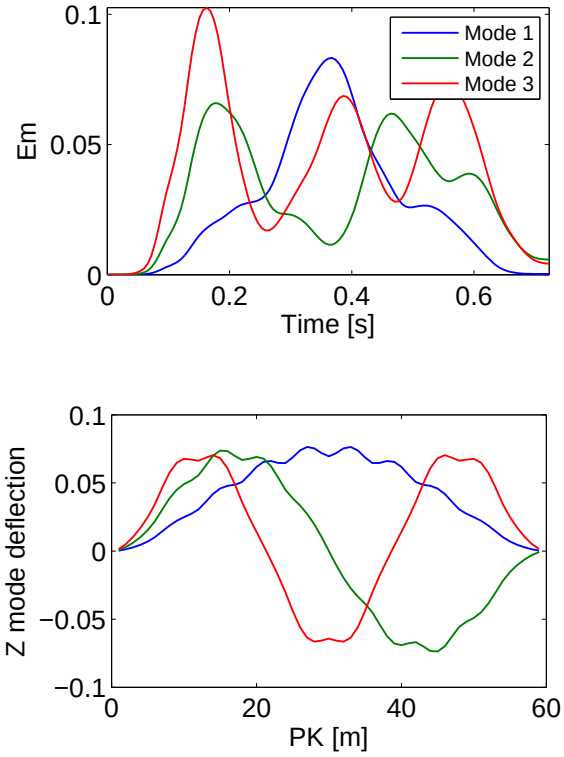

Figure 2: First 3 modal energies for a time simulation compared to the first 3 modes z deflection.

Classification of the vertical modes can also be interesting. Figure 3 illustrates the maximum of Em response for each exited mode. The highest energies are found at low frequencies, with maximum for mode 13 at 7.2 Hz. The energy then decreases regularly. The max(Em) curve illustrates that the energy input into a mode is associated to a match between wavelength and pantograph speed.

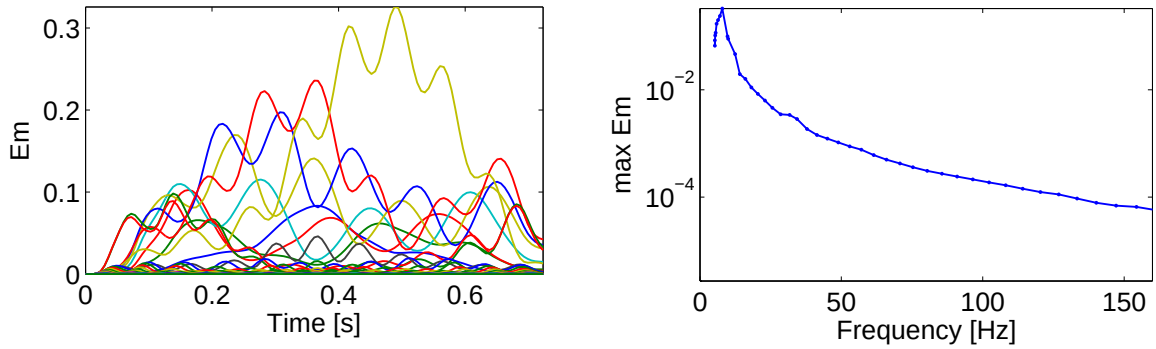

Figure 3: When pantograph is sliding under the wire. Left: modal energies. Right: Max of Em.

Once the pantograph leaves, the wire becomes free and modal energies decrease, and one will seek to verify the ability to use modal coordinates to estimate damping ratio. The *Logarithmic Decrement* method is classically used for single mode systems. Measuring the decrease of two successive peaks in the modal amplitude one deduces damping ratio for sub-critical systems.

To eliminate peak detection difficulties, it is proposed here to track the modal energies. Considering a given modal amplitude $\alpha_j(t)$ the free response to an initial condition is that of a single DOF mass/stiffness/damper

system with

$$m = 1, k = \omega_j^2, c = \phi_j^T C \phi_j = 2\zeta_j \omega_j \tag{16}$$

and dynamic equation

$$\ddot{\alpha}_j(t) + 2\zeta_j \omega_j \dot{\alpha}_j(t) + \omega_j^2 \alpha_j(t) = 0 \tag{17}$$

whose characteristic equation has discriminant $\Delta = 4\omega_j^2(\zeta_j^2 - 1)$.

Sub-critical damping is found for $\zeta_j < 1$ (negative discriminant). There are two conjugate poles $\lambda = \omega_j(-\zeta_j \pm \imath\sqrt{1-\zeta_j^2})$ and a time response of the form $\alpha_j(t) = A_j \cos(\omega_j\sqrt{1-\zeta_j^2}t + \theta_j)\exp(-\zeta_j\omega_j t)$ where A_j and θ_j are two constants depending on initial conditions. Modal energy can be computed using (15) and is of the form

$$Em_j(t) = (A + f(t))\exp(-2\zeta_j\omega_j t)$$

where $f(t) << A$ (f is composed of $\sin^2$, $\cos^2$ and $\sin\cos$ products that explains minor oscillations).

The energy decrease in a log scale plot is thus a straight line showing minor oscillations and can be estimated with a simple curve fit which gives an estimate of modal damping.

Critical damping is found for $\zeta_j = 1$. The system then has a double pole $\lambda = -\omega_j$ and a time response of the form $(A_j + B_j t)\exp(-\omega_j t)$ where A_j and B_j are two constants depending on initial conditions. Modal energy is of the form $Em_j(t) = P(t)\exp(-2\gamma_j t)$ where P is a second order polynomial.

Supercritical damping is found for $\zeta_j > 1$. Then there are two real poles $\lambda = \omega_j(-\zeta_j \pm \sqrt{\zeta_j^2 - 1})$ and a time response $\alpha_j(t) = (A_j\exp(\omega_j\sqrt{\zeta_j^2-1}t) + B_j\exp(-\omega_j\sqrt{\zeta_j^2-1}t))\exp(-\zeta_j\omega_j t)$ where A_j and B_j are two constants depending on initial conditions. The exponential associated with the lowest frequency pole decreases much more slowly so that the modal energy takes the form $Em_j(t) \approx (A + f(t))\exp(-2\omega_j(\zeta_j - \sqrt{\zeta_j^2-1})t)$ where f is small compared to A.

From the decay of modal energies $log(Em_j)$, shown in figure 4, a simple least square methods was used to estimate the exponential constant γ_j (ζ_j for sub-critical damping and $\zeta_j - \sqrt{\zeta_j^2 - 1}$ for supercritical damping). One clearly finds the theoretical behavior for Rayleigh damping of a linear increase up to critical damping and a decrease of γ_j above that threshold.

The low frequency at which critical damping occurs is a property of Rayleigh damping that is rarely discussed. In the present application, it implies that wave propagation can only be studied at frequencies much below that limit. Explaining the variations in estimated damping around critical damping would be interesting.

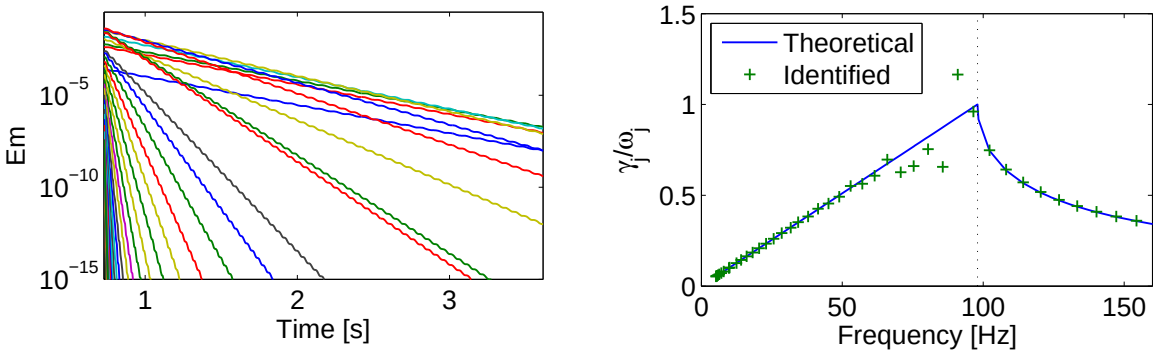

Figure 4: When wire is free. Left: modal energies in ylog. Right: Identified γ_j/ω_j.

In order to validate the implementation of modal damping in SDT, two passage simulations with and without modal damping are compared. In the second, a modal damping of 50 % is added to mode 3 only in addition to the initial Rayleigh damping. The total damping ratio expected on mode 3 is thus $\frac{\beta}{2}\omega_3 + 0.5 = 55.5\%$. For other modes, the $\frac{\beta}{2}\omega_j$ value remains unchanged. From the decay a value of 55.37% (relative error of 0.24 %) is found for mode 3. For other modes the maximum relative error is 0.2%. During the passage, figure 5 shows that modal energy remains almost unchanged for mode 2 and 4, and only changes for mode 3. The figure 5 also shows that damping ratio of mode 3 does not impact the response a lot since the modal energy only decreases by 56% whereas modal damping has increased by a 9 factor.

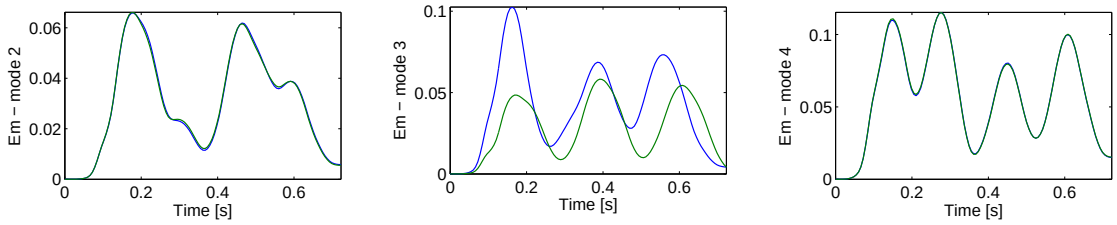

Figure 5: When pantograph is sliding, time evolution of the energies for modes 2, 3 and 4. Blue: nominal Rayleigh damping. Green: nominal+modal damping ratio of 50% added to mode 3.

3.2 Impact test on a real catenary

A significant objective of using modal damping in transient analysis is to introduce a simple mechanism to control damping related system behavior. In catenaries, impact or drop tests can be used to verify global behavior and will be discussed here.

The SNCF LN2 catenary, shown in figure 6, is considered with an *Initial* piecewise Rayleigh damping proportional to stiffness ($\beta_{CW} = 3.25e-3$, $\beta_{MW} = 1.75e-2$, $\beta_{dropper} = 1.5e-8$ and every $\alpha_e = 0$). These values are not optimal in many respects.

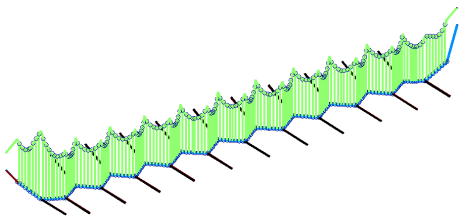

Figure 6: LN2 catenary (transverse dimensions with a 100 scale)

One first seeks to illustrate implications of (8) (the MSE method). Figure 7 (right) shows the fraction of energy in the contact wire (CW) or in the messenger wire (MW), distinguishing between compression (A), bending (I1), torsion (J), and pretension (ten). For most of the modes the major part of elastic energy is pretension energy (ten). Some modes are mostly localized in the CW or in the MW (when energy fraction of the component is near 1). For these modes, the damping ratio, shown left in the figure, match the damping ratio of the component where the energy is localized.

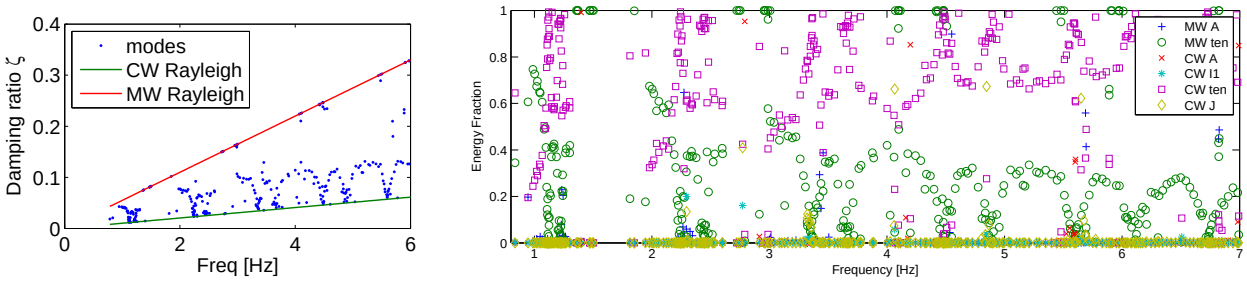

Figure 7: LN2 catenary, initial piece-wise Rayleigh damping (*Initial*). Left: Modal damping ratios. Right: Strain energy fraction for each mode.

For impact tests, frequency and time domain analyses can easily be compared. From the time domain analysis, a transfer is obtained as ratio of response and force input spectra. The results shown in figure 8 correlate perfectly at low frequencies. Differences at higher frequencies are attributed to the periodicity error induced by the mean acceleration Newmark scheme.

The response shows peaks for the first four groups of modes at 1 Hz, 2 Hz, 3 Hz and 4 Hz (first and second group vertical modes correspond respectively mainly to first and second span modes). Within each group, individual modal resonances cannot be separated. The *Initial* damping model is thus too damped. Frequencies higher than 4 Hz are not seen, and modes are not clearly separated.

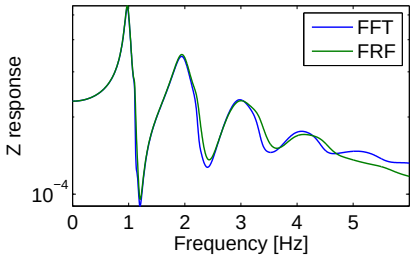

Figure 8: LN2 catenary, *Initial* piece-wise Rayleigh damping. FFT (blue) and FRF (green).

Tests can be used to obtain a physical reference for such response. In this study, one will take this reference to be a modal damping of 1% on modes below 3.5 Hz. For higher modes, Rayleigh damping is still used but coefficients are decreased to have 1% at 3.5 Hz on the contact wire. Values are shown in figure 9 (left). This damping model will be called *Modal* in the rest of the study.

The first mode groups now show individual peaks (as seen in figure 9 - right) and CW modes only reach 5% damping at 17.5 Hz.

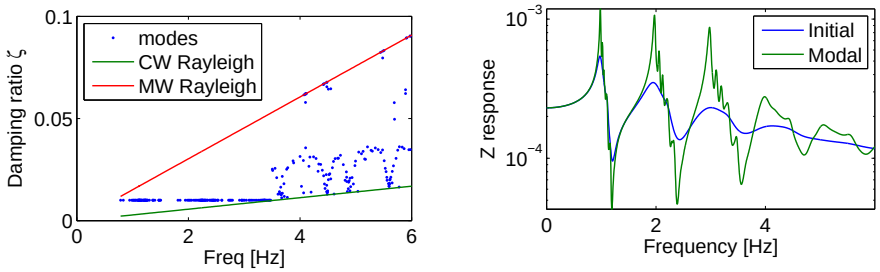

Figure 9: LN2 catenary. Left: modal damping ratios (*Modal*). Right: FRF for *Initial* (blue) and *Modal* (green) damping models.

When imposing 1% on modes whose frequency is lower than 3.5 Hz the adjusted piece-wise Rayleigh damping applied everywhere is compensated: corresponding damping ratios estimated by $diag([\Phi]^T C[\Phi])$ are removed from target damping ratios. This can lead, without problem, to negative modal damping ratio in the modal damping contribution.
Extra-diagonal terms are neglected when compensating piece-wise Rayleigh damping since $[\Phi]^T[C][\Phi]$ is not diagonal in that case. Figure 10 shows color map of the projection of the piece-wise Rayleigh damping on the first 50 modes corresponding to $\frac{\|c_{ij}\|}{\sqrt{c_{ii}c_{jj}}}$ and corresponding histogram. Most of the extra-diagonal terms are lower than 0.05 and none of them exceed 0.4, this implies that effects of non proportional damping are small [5].

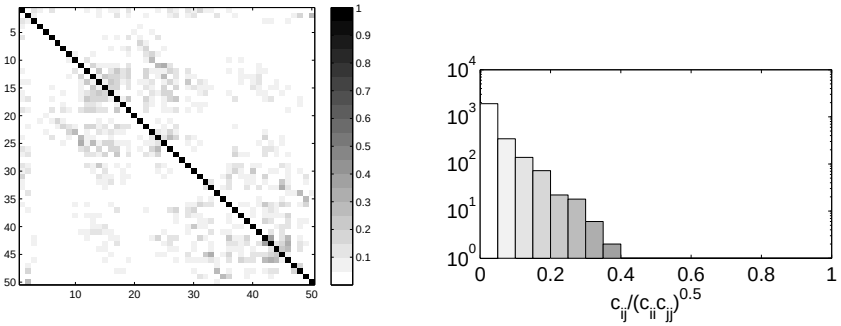

Figure 10: $\frac{c_{ij}}{\sqrt{c_{ii}c_{jj}}}$ for the first 50 modes. Left : color map. Right : histogram (scale log).

3.3 OSCAR time simulation

The same LN2 catenary is now considered in a full OSCAR time simulation. A simple pantograph, composed of 3 mass/stiffness/damper stages, is added. The time simulation corresponding to the passage of the pantograph at a speed of 83 m/s with a mean contact force of 170N is analyzed.

Figure 11 compares the contact force for the *Initial* (piece-wise Rayleigh damping) and *Modal* (adjusted Rayleigh for f >3.5Hz + modal damping 1% for f <3.5Hz) models of section 3.2. The contact force mostly shows the excitation seen by the pantograph: dropper periodicity, span periodicity etc. at current speed. In the figure, the main peak is associated with dropper repetition (distance between droppers at a train velocity of 83 m/s correspond to frequencies around 1.6 Hz as shown in gray in the FFT).

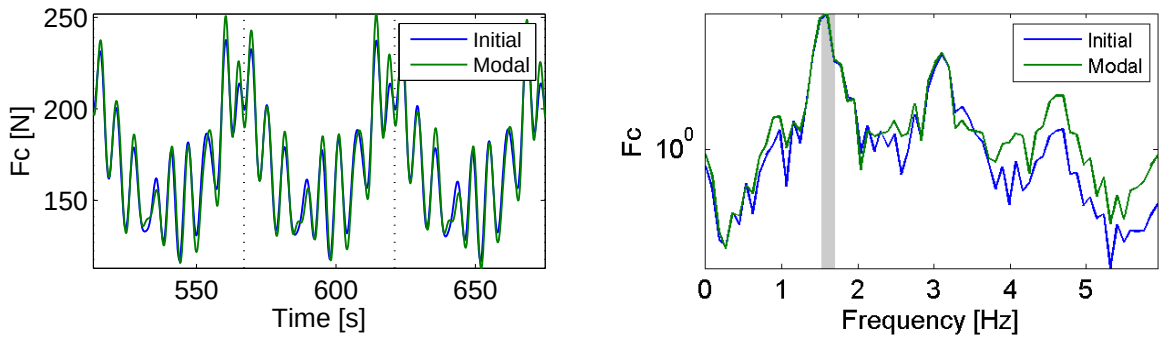

Figure 11: Contact force. LN2 catenary, *Initial* (blue) and *Modal* (green) damping models.

The uplift measured at the middle of the catenary is shown in figure 12 and is more sensitive to damping. With modal damping, residual vibration after the pantograph passage is significantly more accurate. The spectrum is comparable to the impact spectrum shown in section 3.2, so that the influence of modal damping is not a surprise.

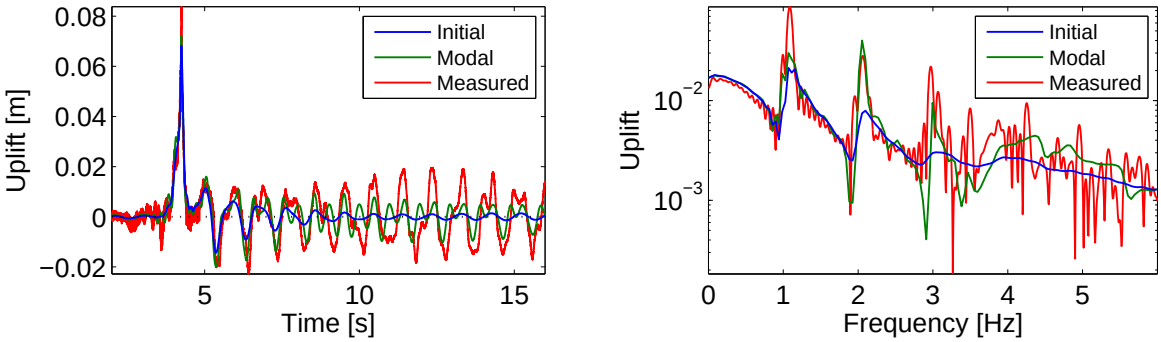

Figure 12: Uplift at the middle of the catenary. LN2 catenary, *Initial* (blue) and *Modal* (green) damping models compared to measurement (red).

The *Modal* model with 1% damping shows better correlation for the peaks at 2Hz, 3 Hz and 4 Hz. The first resonance is however not predicted properly. It was seen in section 3.1, that the moving load and low frequencies are important driver factors in the level of a given resonance. In this case, reducing the damping ratio from 1% to 0.02% around 1 Hz has almost no impact. The ability to control modal damping can thus be used to analyze the influence of various factors.

The numerical cost of transient modal damping is directly associated with the number of retained modes. Modal energies provide a simple mechanism to target modes that have no influence. Figure 13 illustrates modes that don't excite contact wire or have horizontal contact wire motion. A second simulation retaining 133 modes out of 185 shows nearly identical results in figure 13 (the contact force relative error is 8.9e-3 % and uplift relative error is 0.17 %). For the same precision, a 22.6% decrease of CPU time (49.5s to 38.3s for 2000 time steps) is obtained.

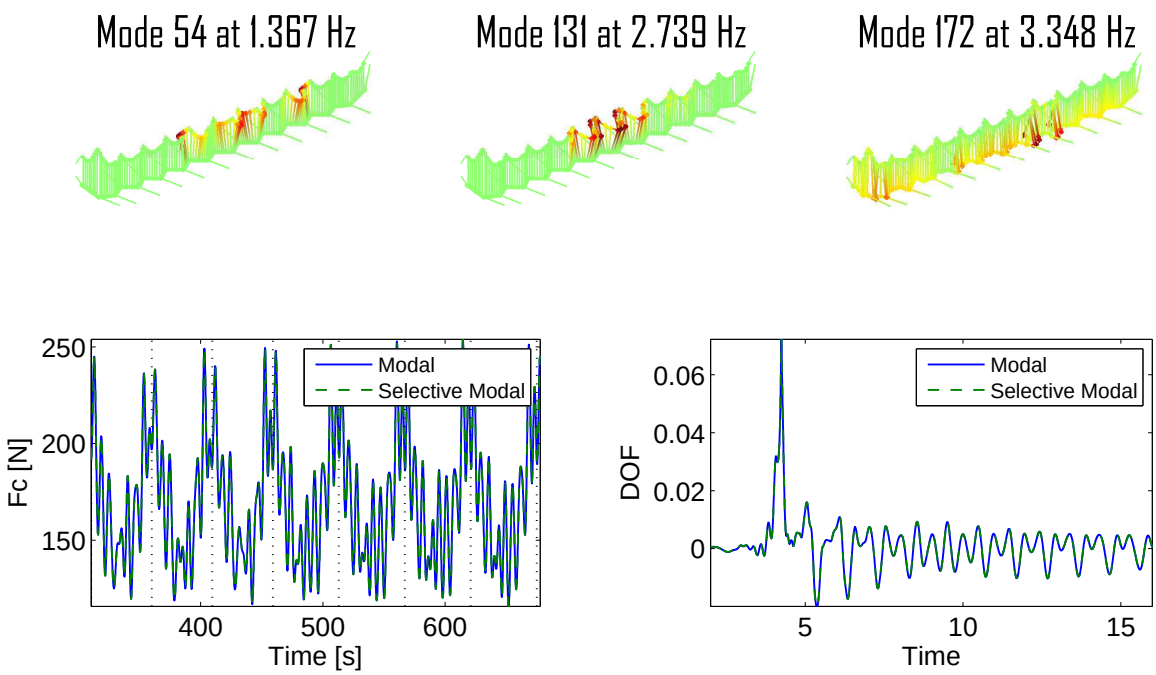

Figure 13: Top: some unkept modes. Down left: contact force. Down right: uplift at the middle of the catenary.

Table 1 shows that time added for residual computation by the modal damping (comparing to *Initial* residual) is proportional to the number of retained modes. Selection of target modes to be damped is thus an important aspect of the proposed methodology.

Damping model	Total time [s]	Residual computation time [s]
Initial	39.4	9.73
Selective *Modal* (133 modes)	68.7	38.28
Modal (185 modes)	80.2	49.49

Table 1: Computation time for 2,000 steps of time

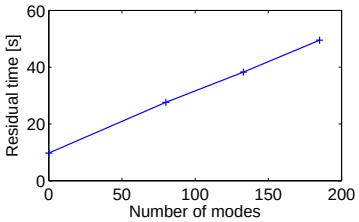

Figure 14: Residual computation time.

Finally, uplift is not necessarily the response most sensitive to damping. For fatigue analysis, the amplitude between the maximum and the minimum stress at a given point is more appropriate. Stress is linked to curvature by

$$\sigma = Ez\kappa \tag{18}$$

where E is the Young modulus, z the distance to the neutral fiber and κ the curvature. Extracting the observation matrices for curvature at integration points, one can compute stresses at the wire surface where

it is maximal. Figure 15 compares stresses and uplifts for the two damping models. Stress is clearly more sensitive to damping with a 50 % increase of stress levels at lower damping.

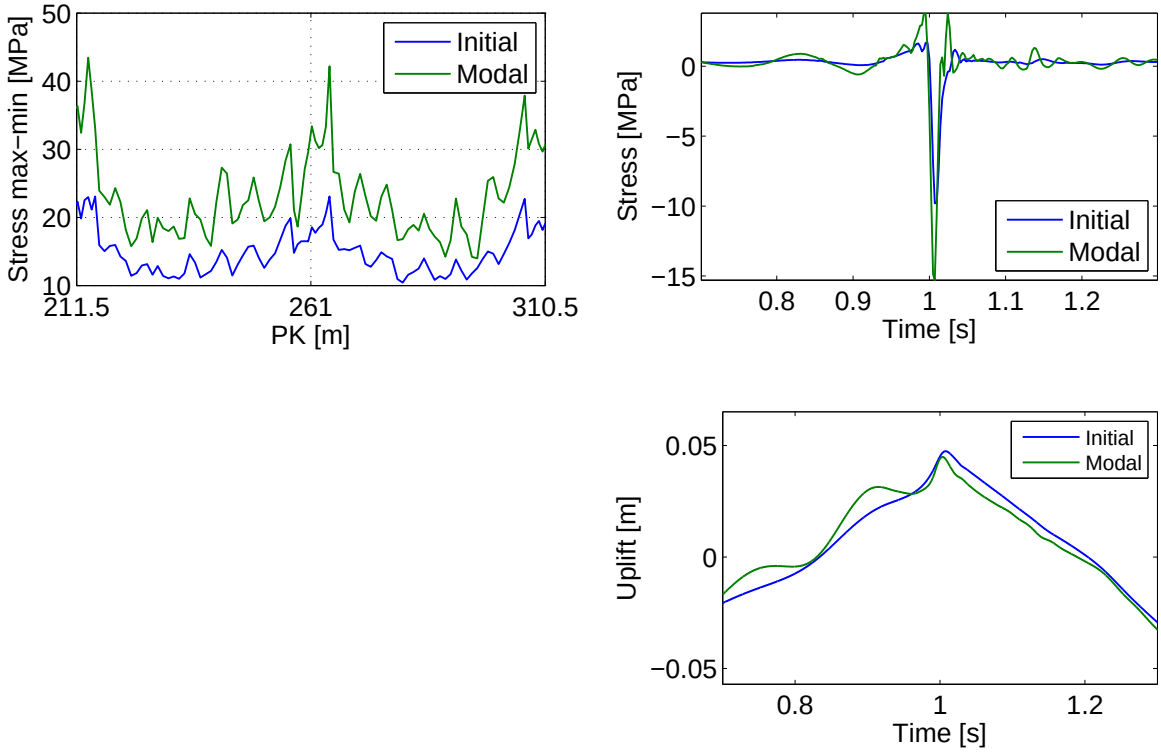

Figure 15: LN2 catenary, *Initial* (blue) and *Modal* (green) damping models. Top: stress criteria and stress at PK=206m when pantograph is passing. Down: Uplift at PK=206m.

4 Conclusion

Modal damping was shown to be a practical tool that can be used to analyze systems showing complex transient behavior that requires time domain integration. The concept is directly linked to the use of modal amplitudes that can also be used to post-process classical transients. The proposed procedure has been used here to diagnose the impact of damping in simulations, which is rarely done in detail. In Ref. [9] the same concept was used as a design tool.

References

[1] C. Bert, "Material damping: An introductory review of mathematical models, measures, and experimental techniques," *Journal of Sound and Vibration*, vol. 29, no. 2, pp. 129–153, 1973.

[2] A. Nashif, D. Jones, and J. Henderson, *Vibration Damping*. John Wiley and Sons, 1985.

[3] E. Balmes, *Viscoelastic vibration toolbox, User Manual*. SDTools, 2004-2009.

[4] M. Géradin and D. Rixen, *Mechanical Vibrations. Theory and Application to Structural Dynamics.* John Wiley & Wiley and Sons, 1994, also in French, Masson, Paris, 1993.

[5] E. Balmes, "New results on the identification of normal modes from experimental complex modes," *Mechanical Systems and Signal Processing*, vol. 11, no. 2, pp. 229–243, 1997.

[6] T. Caughey, "Classical normal modes in damped linear dynamic systems," *ASME J. of Applied Mechanics*, pp. 269–271, 1960.

[7] T. Hasselman, "Modal coupling in lightly damped structures," *AIAA Journal*, vol. 14, no. 11, pp. 1627–1628, 1976.

[8] L. Rogers, C. Johson, and D. Keinholz, "The modal strain energy finite element method and its application to damped laminated beams," *Shock and Vibration Bulletin*, vol. 51, 1981.

[9] G. Vermot des Roches, E. Balmes, R. Lemaire, and T. Pasquet, "Designed oriented time/frequency analysis of contact friction instabilities in application to automotive brake squeal," in *Vibrations, Chocs & Bruit (VCB XVIIth symposium)*, 2010.